THERMAL PERFORMANCE ANALYSIS OF ORGANIC FLASH CYCLE USING R600a/R601a MIXTURES WITH INTERNAL HEAT EXCHANGER

by

Guidong HUANG[a], Songyuan ZHANG[b], Zhong GE[a,*], Zhiyong XIE[a], Zhipeng YUAN[a], Chong TANG[a], Jianbin XIE[a], and Jian XU[a]

[a] School of Architecture and Urban Planning, Yunnan University, Kunming, China
[b] School of Metallurgy and Mining, Kunming Metallurgy College, Kunming, China

Original scientific paper
https://doi.org/10.2298/TSCI200507296H

In this study, the thermal performance of an internal heat exchanger-organic flash cycle system driven by geothermal water was investigated. The R600a/R601a mixtures were selected as the working fluid. The effects of the mole fraction of mixtures on the heat absorption capacity of the heater, the temperature rise of cold working fluid in the internal heat exchanger, net power output, thermal efficiency, and electricity generation costs were analyzed. The net power outputs, electricity generation costs, and thermal efficiency of the internal heat exchanger-organic flash cycle and simple organic flash cycle systems were compared. Results showed that the system using the R600a/R601a mixtures (0.7/0.3 mole fraction) has the largest net power output, which increased the net power output by 3.68% and 42.23% over the R601a and R600a systems, respectively. When the R600a mole fraction was 0.4, the electricity generation costs reduction of the internal heat exchanger-organic flash cycle system was the largest (1.77% compared with the simple organic flash cycle system). The internal heat exchanger can increase the thermal efficiency of organic flash cycle, but the net power output does not necessarily increase.

Key words: *organic flash cycle, internal heat exchanger, zeotropic mixtures, thermal efficiency*

Introduction

The large-scale consumption of fossil fuel has led to the destruction and pollution of the global ecological environment [1-3]. To reduce pollution and the consumption of fossil fuel, the utilization and development of clean energy have become particularly important [4]. Geothermal water is obtained from the depths of the earth. It has been widely studied due to its advantages of large reserves, thermal stability, and no pollution [5, 6]. However, low-temperature geothermal resources are difficult to use.

The organic flash cycle (OFC) is a novel power generation technology that uses low-boiling-point organic fluids. It can effectively convert low- and medium-temperature heat into power [7-10]. Ho *et al.* [11] compared the thermal utilization efficiency of 10 aromatic hydrocarbons and siloxanes for simple OFC and organic Rankine cycle (ORC). They found that the utilization efficiency of aromatic hydrocarbons for simple OFC was 5-20% greater than that

* Corresponding author, e-mail: zhongge@hotmail.com

of optimized ORC. Varma *et al.* [12] used R124 as working fluid to study the influence of pressure changes of heat recovery vapor generator on the power and exergy efficiency of the OFC and ORC systems. They found that when the heat recovery vapor generator's pressure is 15.05-23.99 bar, the increments of power and exergy efficiency of the OFC system are 0.06-14.37% and 0.14-14.47% higher than those of the ORC system, respectively. Li *et al.* [13] compared the total heat transfer coefficient of heat exchanger between the OFC and ORC systems by using R245fa as working fluid. The results showed that when the evaporation temperature was 129-152 °C, the total heat transfer coefficient of the OFC system was greater than that of the ORC system. When the evaporation temperature was 145.19 °C, the total heat transfer coefficient of the OFC system was the highest, which was 22.25% higher compared with that of the ORC system. Kishimoto *et al.* [14] analyzed the recovery efficiency of a simple OFC for low- and medium-temperature waste heat. Mondal *et al.* [15] conducted a thermal performance and economic analysis on the simple OFC system with R245fa/R600a mixtures to utilize low- and medium-temperature exhaust gas without SO_2. They found that the simple OFC system has a significant effect on improving the recover efficiency of low- and medium-temperature exhaust gas. In summary, the simple OFC system can effectively utilize low- and medium-temperature heat source.

At present, several researchers are studying the pure working fluid for simple OFC. The match between cycle and heat source and cold source is poor due to its isothermal phase change characteristics [16, 17]. Zeotropic mixtures have been used to improve temperature matching due to their non-isothermal phase change characteristic in two-phase condensation region. They can further improve the match between the cycle and the heat source and the cold source to improve the system's efficiency [18, 19]. Zhu *et al.* [20] used R245fa/R601a mixtures as working fluid and studied the effects of different evaporation temperatures and composition proportions on the performance of ORC. The results showed that when the R245fa/R601a mole fraction was 0.4/0.6, the R245fa/R601a system had the largest net power output, and the thermal efficiency was approximately 9%. Li *et al.* [21] compared the effects of R245fa and R245fa/R601a on the ORC performance through experimental tests. They found that the thermal efficiency and optimal dimensionless volume ratio of the R245fa/R601a system were greater than those of the R245fa system. In another study, they investigated the performance of the ORC system using R600a/R601a mixtures driven by geothermal water at 100-200 °C. The results showed that when the heat source temperature was 100-160 °C and 180-200 °C, the net power output of the R600a/R601a system was greater than that of the pure working fluid system [22]. Wang *et al.* [18] conducted an experimental analysis of the R600a/R601a ORC system at a constant temperature (115 °C). They observed that the maximum net power output of the R600a/R601a system was relatively increased by 71% and 25% compared with the R600a and R601a systems, respectively. In summary, zeotropic mixtures can effectively improve the ORC system's performance.

At present, many researchers use an internal heat exchanger (IHE) to improve system performance [23-25]. Lu *et al.* [26] studied the thermal performance of an IHE-ORC system utilizing zeotropic mixtures. The results showed that the IHE can effectively improve the system's efficiency. The IHE absorbs the exhaust vapor from the turbine to heat the cold fluid at the feed pump outlet, which can effectively increase the working fluid temperature at the heater inlet, reducing the heat loss in the heating process [27, 28]. Therefore, to further improve the system's performance, this study utilized zeotropic mixtures and IHE.

At present, researchers mainly focus on improving the performance of the simple OFC system. When an IHE is introduced in the OFC system, its effects on net power output,

thermal efficiency, and electricity generation costs (EGC) are uncertain. Furthermore, when zeotropic mixtures are introduced into the IHE-OFC system, the effects of working fluid mole fraction on the net power output, thermal efficiency, and EGC of the IHE-OFC system remain to be elucidated. Because two-phase zeotropic mixtures are separated from the vapor separator, the mole fractions of the saturated vapor and saturated liquid are not consistent with those of the original fraction.

In the present study, an IHE-OFC system utilizing zeotropic mixtures was proposed. R600a and R601a are used as the working fluid due to their environmental friendliness, low cost, and stability [22, 29, 30], and many scholars have studied the thermal performance of system using R600a and R601a [1, 19, 31]. The thermal properties of the working fluids are shown in tab. 1. A thermodynamic model of the IHE-OFC system was established. The effects of the mole fractions of mixtures on the heat absorption capacity of the heater, temperature rise of cold working fluid in the IHE, net power output, thermal efficiency, and EGC were studied under optimal operating parameters. The net power output, thermal efficiency, and EGC of simple OFC and IHE-OFC were compared.

Table 1. Working fluid parameters [22, 29, 30]

Working fluid	Molecular mass [g/mol]	Fluid type	Critical temperature [°C]	Critical pressure [MPa]	GWP	ODP
R600a	58.12	Dry fluid	134.7	3.63	~20	0
R601a	72.15	Dry fluid	187.2	3.38	~20	0

Calculation model of the IHE-OFC system

The HE-OFC system

In the present study, the IHE-OFC system utilizing zeotropic mixtures and *T-s* diagram are shown in figs. 1 and 2, respectively. The organic working fluid coming out of the heater – 2, 3, after undergoing high-pressure throttle valve – 3, 4, enters into the vapor separator to achieve gas-liquid separation – 4, 5, 8. Dry saturated vapor is discharged from the top of the separator into the turbine and expands – 5, 6. The exhaust vapor is discharged from the turbine and enters into the hot fluid side of the IHE – 6, 10. The saturated liquid flows out from the bottom of the separator and is throttled by a low-pressure throttle valve – 8, 9. The

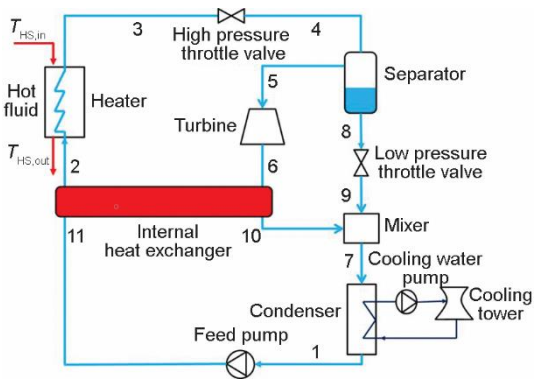

Figure 1. The IHE-OFC system diagram

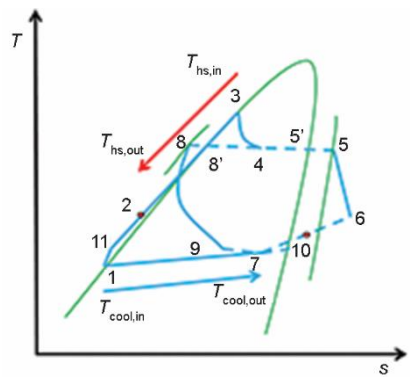

Figure 2. The *T-s* diagram of mixtures IHE-OFC system

exhaust vapor discharged from the hot fluid side of the IHE is mixed with the throttled saturated liquid in the mixer – 9, 10, 7, and enters into the condenser – 7, 1. After undergoing a condensation process, the working fluid is pressurized to the cold fluid side of the IHE pressure – 1, 11. The working fluid comes out of the cold fluid side at the IHE outlet and enters into the heater – 2, 3, to form a cycle.

Basic assumptions are:

– The IHE-OFC is in stable operation.
– The entropy efficiency of the feed pump and turbine is constant.
– The pressure drops and heat loss of the heat exchanger and pipes are ignored.

Thermodynamic calculation models

In the heating process, the basic equation of the thermal equilibrium is:

$$Q_{\text{sys}} = \dot{m}_{\text{HS}}(h_{\text{HS,in}} - h_{\text{HS,out}}) = \dot{m}_{\text{f}}(h_3 - h_2) \tag{1}$$

where $\dot{m}_{\text{f}}$ is the mass-flow rate of the working fluid and calculated:

$$\dot{m}_{\text{f}} = \frac{\dot{m}_{\text{HS}}(h_{\text{HS,in}} - h_{\text{HS,out}})}{h_3 - h_2} \tag{2}$$

The mass-flow rate of the vapor and liquid is:

$$\dot{m}_{\text{v}} = x\dot{m}_{\text{f}} \tag{3}$$

$$\dot{m}_l = (1 - x)\dot{m}_{\text{f}} \tag{4}$$

where x is the vapor dryness and calculated:

$$x = \frac{h_4 - h_8}{h_5 - h_8} \tag{5}$$

Due to the non-isothermal phase change characteristics of zeotropic mixtures on the condensation process, the condensation dew point temperature may occur in the IHE or condenser. Thus, when the condensation dew point temperature is in the IHE, the basic equation of the thermal equilibrium is:

$$\dot{m}_{\text{v}}\left(h_6 - h_{\text{dew}}\right) = \dot{m}_{\text{f}}(h_2 - h_{\text{IHE,cw}}) \tag{6}$$

When the condensation dew point temperature is in the condenser, the basic equation of the thermal equilibrium is:

$$Q_{\text{IHE}} = \dot{m}_{\text{v}}(h_6 - h_{10}) = \dot{m}_{\text{f}}(h_2 - h_{11}) \tag{7}$$

The total power output of the turbine is:

$$W_{\text{T}} = \dot{m}_{\text{v}}(h_5 - h_6) \tag{8}$$

The power consumption of the cooling water pump is:

$$W_{\text{cool}} = \frac{\dot{m}_{\text{cool}} g H}{\eta_{\text{cool}}} \tag{9}$$

Due to the non-isothermal phase change characteristics of mixtures, a temperature glide phenomenon occurs during the condensation process, and the position of the pinch point

temperature difference is indeterminate. In the present study, the condensation process is divided into 20 small sections for calculation. The calculation formula of $\dot{m}_{\text{cool}}$ is:

$$\dot{m}_{\text{cool}} = \frac{\dot{m}_{\text{f}}(h_7 - h_1)}{h_{\text{cool,out}} - h_{\text{cool,in}}} \tag{10}$$

where $\dot{m}_{\text{cool}}$ is the mass-flow rate of cooling water.

The power consumption of the feed pump is:

$$W_{\text{p}} = \dot{m}_{\text{f}}(h_{11} - h_1) \tag{11}$$

The net power output of the system is:

$$W_{\text{net}} = W_{\text{T}} - W_{\text{p}} - W_{\text{cool}} \tag{12}$$

The thermal efficiency of the system is:

$$\eta_{\text{sys}} = \frac{W_{\text{net}}}{Q_{\text{sys}}} \tag{13}$$

Thermoeconomic analysis

In the present study, the heater, condenser, and heat exchanger are divided into 20 sections, and the working fluid temperature and thermophysical parameters can be determined by each section.

The heat transfer area of each section is:

$$A_{\text{i}} = \frac{Q_{\text{i}}}{U_{\text{i}}\Delta T_{\text{m,i}}} \tag{14}$$

where U_{i} is the overall heat transfer coefficient, its calculation equation is shown in eq. (15), $\Delta T_{\text{m,i}}$ is the logarithmic mean temperature difference of each section, its calculation equation is shown in eq. (16):

$$\frac{1}{U_{\text{i}}} = \frac{1}{\alpha_{\text{i}}}\frac{d_{\text{o}}}{d_{\text{i}}} + R_{\text{i}}\frac{d_{\text{o}}}{d_{\text{i}}} + R_{\text{o}} + \frac{\delta_{\text{wall}}}{\lambda_{\text{wall}}}\frac{d_{\text{o}}}{d_{\text{m}}} + \frac{1}{\alpha_{\text{o}}} \tag{15}$$

where α_{i} and α_{o} are the convection heat transfer coefficients inside and outside the heat exchanger tube, respectively, d_{i}, d_{o}, and d_{m} are the internal, outside, and average diameters of the heat exchanger tube wall thickness of the heat exchanger, respectively, δ_{wall} is the tube thickness, R_{i} and R_{o} are the internal and outside tube fouling resistance, respectively, and λ_{wall} is the tube wall thermal conductivity, which is 380 kW/mK:

$$\Delta T_{\text{m,i}} = \frac{\Delta T_{\text{max,i}} - \Delta T_{\text{min,i}}}{\ln\dfrac{\Delta T_{\text{max,i}}}{\Delta T_{\text{min,i}}}} \tag{16}$$

where $\Delta T_{\text{max,i}}$ and $\Delta T_{\text{min,i}}$ are the maximum and minimum heat exchange differences of each section, respectively.

The purchased equipment costs (PEC) of the heater, condenser, IHE, turbine, and feed pump were calculated:

$$PEC = 10^{[K_1 + K_2 \log_{10} Y + K_3 (\log_{10} Y)^2]} \tag{17}$$

where the parameters K_1, K_2, and K_3 are listed in tab. 2 [31] and Y is the heat exchange area of the heater, condenser, and IHE or the power of turbine and feed pump.

The annual capital cost (ACC) is calculated:

$$ACC = 6.32\sum_k PEC_k \left[\frac{i(1+i)^n}{(1+i)^n - 1}\right] \tag{18}$$

where i is the interest rate (5%) and n is the system's economic life (20 years).

The annual operation and maintenance cost (AOC) is calculated:

$$AOC = 0.2\sum_k PEC_k \tag{19}$$

The EGC of the system are calculated:

$$EGC = \frac{ACC + AOC}{W_{\text{net}}\tau_{\text{OH}}} \tag{20}$$

where τ_{OH} is the annual operating hours (7500 h).

Table 2. Parameters for the calculation of PEC [31]

Component	Y [unit]	K_1	K_2	K_3
Heat exchanger	Area [m^2]	4.3247	–0.3030	0.1634
Turbine	Power [kW]	2.6259	1.4398	–0.1776
Feed pump	Power [kW)	3.3892	0.0536	0.1538

Model verification

To verify the accuracy of the model in the present study, the calculation results were compared with those in [32]. The boundary conditions were consistent with those in [32]. The comparison results are listed in tab. 3. The maximum relative errors of vapor dryness, x, and specific enthalpy at the turbine inlet, h_5, are 1.21% and 0.08%, respectively. Thus, the model is accurate.

Table 3. Comparison of the results of the present study and [32]

Butane							
T_3	P_F [MPa]	x		Relative error	h_5 [kJkg^{-1}]		Relative error
		Present study	[32]		Present study	[32]	
413	1.2	0.623	0.628	0.80%	707.13	706.55	0.08%
	1.4	0.569	0.575	1.04%	716.27	715.79	0.07%
	1.6	0.517	0.522	0.96%	724.01	723.63	0.05%
	1.8	0.464	0.469	1.07%	730.53	730.28	0.03%
	2.0	0.409	0.414	1.21%	735.98	735.85	0.02%

Relative error = |present study – [32]|/ [32] × 100%

Results and discussion

In the present study, the R600a/R601a mixtures were utilized as the working fluid. The thermophysical properties of the working fluid were obtained from REFPROP 9.0. The thermodynamic model was established by using MATLAB 2019a, and the effects of the changes of mixed fractions on the thermal performance of the system were studied. Table 4 lists the calculation parameters of the IHE-OFC system.

Table 4. Calculation parameter setting

Parameter	Value	Parameter	Value
Geothermal water inlet temperature [°C]	150	Inlet temperature of cooling water [°C]	25
Mass-flow rate [kgs^{-1}]	1	Pinch point temperature difference in heater [°C]	10
Pressure of hot fluid [MPa]	0.5	Pinch point temperature difference in condenser [°C]	5
Isentropic efficiency of turbine [%]	80	Heat transfer temperature difference in IHE [°C]	5
Isentropic efficiency of feed pump [%]	75	Ambient temperature [°C]	15
Efficiency of cooling water pump [%]	85		

As shown in fig. 3, under the optimized operating conditions, the condensation temperature rise initially increases and then decreases with increasing R600a mole fraction, and there are two intersection points with the cooling water temperature rise. At the two intersections, the R600a/R601a mixtures have the best match between the condensation process and the cooling water temperature rise, and the heat loss is minimal. When the R600a mole fraction is 0.4, the condensation temperature rise is maximal.

As shown in fig. 4, the temperature rise of cold working fluid in the IHE ($\Delta T_{\mathrm{IHE,cw}} = T_2 - T_{11}$) initially increases and then decreases with increasing R600a mole fraction. This is because the IHE absorbs the heat of the hot working fluid side to heat the supercooled liquid of the cold working fluid side, and the specific enthalpy difference of the hot working fluid in the IHE increases and then decreases with the increase of R600a mole fraction. According to the energy conservation principle of heat transfer, the specific enthalpy difference of cold working fluid in the IHE increases and then decreases. Thus, the temperature

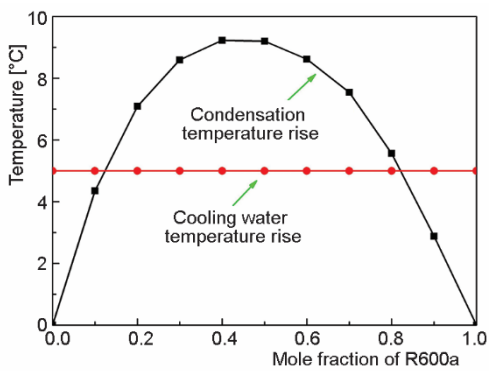

Figure 3. Condensation temperature rise and cooling water temperature rise of R600a/R601a mixtures

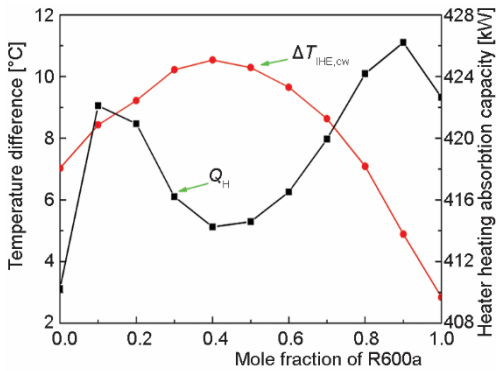

Figure 4. Temperature rise of cold working fluid in the IHE and heat absorption capacity of the heater of R600a/R601a mixtures

rise of the cold working fluid in the IHE increases and then decreases. When the R600a mole fraction is 0.4, the maximum temperature rise of the cold working fluid in the IHE is 10.54 °C. When the R600a mole fraction is 1, the minimum temperature rise of the cold working fluid in the IHE is 2.84 °C. The reason is that the cold fluid side at the IHE inlet temperature is minimal. With increasing R600a mole fractions, the heat absorption capacity of the heater initially increases to the first peak and then decreases and finally increases to the second peak and then decreases. This is because when the heat source temperature is constant, the heat absorption capacity of the heater is mainly affected by the heat source outlet temperature. The heat source outlet temperature initially decreases and then increases and finally decreases and then increases with increasing R600a mole fraction. Thus, the heat absorption capacity of the heater initially increases and then decreases and finally increases and then decreases. When the R600a mole fraction is 0.9, the maximum heat absorption capacity of the heater is 426.21 kW. When the R600a mole fraction is 0, the minimum heat absorption capacity of the heater is 410.24 kW. The heat absorption capacity of the heater presents a valley value (414.25 kW) when the temperature rise of the cold working fluid in the IHE reaches the peak.

Figure 5 shows the changes of the net power output of the system with the flash pressure under different mole fractions. The net power output initially increases and then decreases with increasing flash pressure on the whole. This finding indicates that an optimal flash pressure exists with a maximum net power output at each mole fraction condition. When the mole fraction of the R600a/R601a mixtures is 0.7/0.3 and the flash pressure is 1.41 MPa, the maximum net power output is 26.18 kW. When the mole fraction of the R600a/R601a mixtures is 1.0/0.0 and the flash pressure is 1.64 MPa, the minimum net power output is 18.97 kW.

As shown in fig. 6, the maximum net power outputs of the IHE-OFC and simple OFC initially increase to the first peak and then decrease and finally increase to the second peak and then decrease with increasing R600a mole fraction. This is because there is a temperature glide of the R600a/R601a mixtures during the condensation process, and its changing trend initially increases and then decreases. Moreover, the matching relationship with the cooling water temperature rise becomes better at first and then becomes worse, and better again and then worse (fig. 3). Thus, the net power output initially increases and then decreases and finally increases and then decreases. When the R600a mole fraction is 0.7, the maximum net power output is 26.18 kW. This is because although the R600a mole fraction is 0.8, the match between the condensation temperature rise and the cooling water temperature rise is

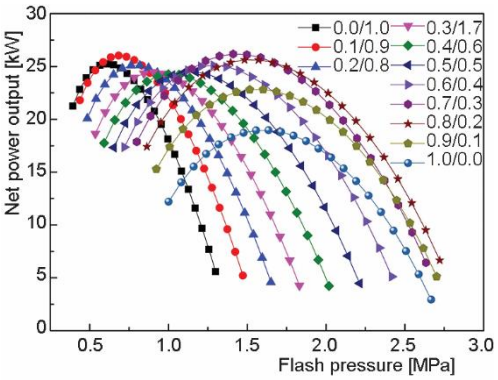

Figure 5. Variation of net power output with flash pressure

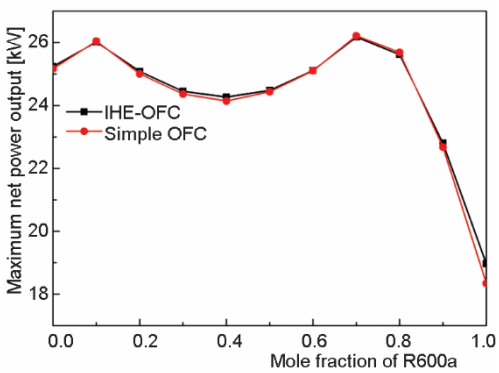

Figure 6. Maximum net power output of R600a/R601a mixtures

well. However, at this time, the heat source temperature is greater than the characteristic temperature of the working fluid (the characteristic temperature of the working fluid is a sum of the pinch point temperature difference of the heater and the temperature corresponding to $0.85P_{cri}$), the temperature difference at the heater outlet ($\Delta T_{H,out} = T_{HS,in} - T_3$) is greater than the pinch point temperature difference, the heat transfer loss increases at this time, and the system throttling loss is larger. Thus, when the R600a mole fraction is 0.7, the net power output is maximal. When the R600a mole fraction is 0, 0.2-0.6, or 0.9-1, the net power output of IHE-OFC is greater than that of simple OFC. When the R600a mole fraction is 0.1 or 0.7-0.8, the net power output of IHE-OFC is less than that of simple OFC.

As shown in fig. 7, under the optimized operating conditions, the thermal efficiency of IHE-OFC initially increases and then decreases and finally increases and then decreases with increasing R600a mole fraction. This is because the thermal efficiency is affected by the heat absorption capacity of the heater and net power output. When the R600a mole fraction is 0.0-0.1, the thermal efficiency of the system increases because the decrement of the heat absorption capacity of the heater is greater than that of the net power output. When the R600a mole fraction is 0.2-1, the thermal efficiency of the system initially decreases and then increases and finally decreases with increasing R600a mole fractions. This is because the net power output initially decreases and then increases and finally decreases. The thermal efficiency of simple OFC initially decreases and then increases and finally decreases with increasing R600a mole fractions. When the R600a mole fraction is 0-0.1, the decrement of the thermal efficiency of system is smaller. This is because although the R600a mole fraction is 0.1, the net power output of the system is a peak value. However, the increment is not large at this time compared with the R601a system, and the heat absorption capacity of the heater is larger. Thus, the thermal efficiency is smaller than that of the R601a system. When the R600a mole fraction is 0.2-1.0, the change of the heat absorption capacity of the heater is unremarkable with increasing R600a mole fraction. The thermal efficiency of the system is mainly affected by the net power output. With increasing R600a mole fractions, the net power output initially decreases and then increases and finally decreases. Thus, the thermal efficiency of the system initially decreases and then increases and finally decreases. Because the IHE increased the working fluid temperature at the heater inlet, the thermal efficiency of the IHE-OFC system is greater than that of the simple OFC system. When the R600a mole fraction is 0.4, the maximum relative increment is 10.98%; when the R600a mole fraction is 1.0, the minimum relative increment is 3.46%.

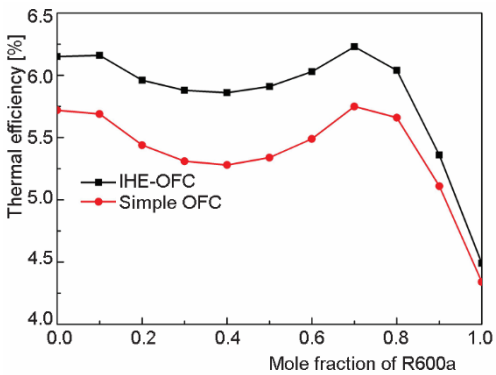

Figure 7. System thermal efficiency of R600a/R601a mixtures

Figure 8 shows the heater and IHE heat transfer areas of IHE-OFC and simple OFC for the optimal operation conditions at various R600 mole fractions. With the increase in R600a mole fraction, the heat transfer area of IHE-OFC and simple OFC first increases and then decreases. As can be seen from fig. 8, the overall heat exchange area of the IHE-OFC system is smaller than that of the simple OFC system. This is because the IHE increases the temperature of the working fluid at the heater inlet and the logarithmic mean temperature dif-

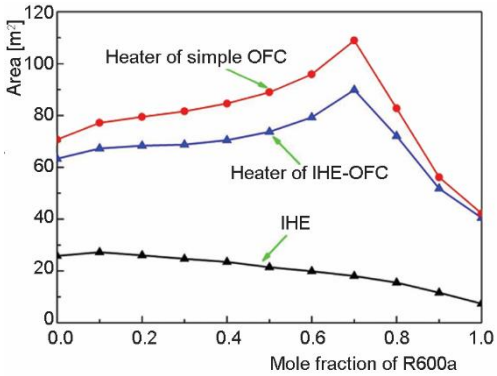

Figure 8. The heater and IHE heat transfer areas of IHE-OFC and simple OFC for the optimal operation conditions at various R600 mole fractions

ference of the heating process, and the heat transfer coefficient also increases correspondingly, which leads to the decrease of the heat transfer area of the IHE. When the R600a mole fraction is 0.7, the heat transfer areas of IHE-OFC and simple OFC are 89.85 and 108.95 m^2, respectively. Moreover, the heat transfer area of the IHE-OFC system is 17.53% less than that of the simple OFC system. When the R600a mole fraction is 1, the heat transfer area of IHE-OFC and simple OFC is the smallest. However, the heat transfer area of IHE-OFC is 3.95% less than that of simple OFC. For R600a/R601a mixtures, when the R600a mole fraction is 0.9, the heater heat transfer areas of the IHE-OFC and simple OFC systems are 20.57% and 18.14% less than those of the R601a system, respectively. For the IHE, when the R600a mole fraction is 0-0.1, the heat transfer area of IHE increases. When the R600a mole fraction is 0.1, the maximum heat transfer area of IHE is 27.24 m^2. This is because the increment of the heat transfer coefficient and logarithm mean temperature difference of IHE are smaller than those of 0 R600a mole fraction, however, the heat absorption increment of IHE is larger, eq. (14). When the R600a mole fraction is 0.2-1, the heat transfer area of IHE decreases. This is because of the increment of the heat transfer coefficient and logarithmic mean temperature difference of the IHE. When the R600a mole fraction is 1, the heat transfer area of the IHE is the smallest, which is reduced by 79.92% compared with the maximum heat transfer area of IHE.

Figure 9 shows the EGC for the optimal operation conditions at various R600 mole fractions. For the R600a/R601a mixtures, the EGC of the IHE-OFC and simple OFC systems are smaller than that of the R600a system when the R600a mole fraction is 0.1-0.9. Moreover, the EGC of the IHE-OFC system is smaller than that of the simple OFC system. When the R600a mole fraction is 0.4, the EGC reduction of the IHE-OFC system is the largest, which is 1.77%. When the R600a mole fraction is 0, the EGC of the IHE-OFC and simple OFC systems are the smallest, and the EGC of the IHE-OFC system is 0.32% larger than that of the simple OFC system. This is because although the net output power of the IHE-OFC system is larger than that of the simple OFC system, its increment is small, and the total heat transfer area of the IHE-OFC system is larger than that of the simple OFC system. Thus, the EGC of the IHE-OFC system is larger. This shows that R601a is more suitable for the simple OFC system in terms of EGC. When the R600a mole fraction is 1, the EGC of IHE-OFC and simple OFC of R601a is the largest, and the EGC of the IHE-OFC system is 2.33% less than that of the simple OFC system.

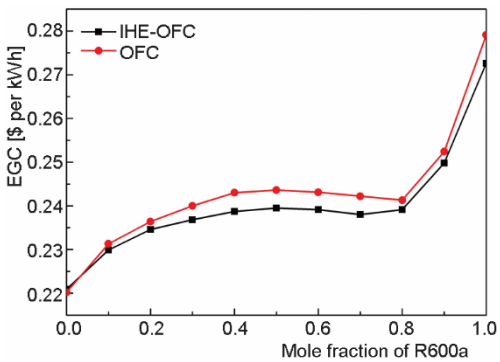

Figure 9. The EGC for the optimal operation conditions at various R600 mole fractions

As shown in tab. 5, the net power outputs of the R600a and R601a systems are 18.97 and 25.24 kW, respectively. The maximum net power output of the R600a/R601a system is 38.00% and 3.72% higher than that of the pure R600a and R601a systems, respectively. The result shows that the heat utilization efficiency was effectively improved when the R600a/R601a mixtures were selected as the working fluid in the IHE-OFC system.

Table 5. Comparison of the maximum net power outputs of the mixture system and the pure working fluid system

Optimized mole fraction R600a/R601a	Maximum net power output [kW]	Net power output R601a [kW]	Net power output R600a [kW]	Relative increment R601a [%]	Relative increment R600a [%]
0.7/0.3	26.18	25.24	18.97	3.72	38.00

Relative increment = |mixture system – pure working fluid system|/pure working fluid system × 100%

Conclusions

The present study established an IHE-OFC system utilizing zeotropic mixtures. The system was driven by 150 °C geothermal water. The effects of mixture fraction on the system's performance were analyzed. The net power outputs, thermal efficiencies, and EGC of IHE-OFC and simple OFC were compared. The main conclusions are as follows.

- With increasing R600a mole fraction, the heat absorption capacity of the heater initially increases and then decreases and finally increases and then decreases. The temperature rise of cold working fluid in the IHE initially increases and then decreases and finally increases and then decreases. When the R600a/R601a mole fraction is 0.4/0.6, the heat absorption capacity of the heater presents a valley value, whereas the temperature rise of the cold working fluid in the IHE reaches a peak value.
- In IHE-OFC, the net power output of the system initially increases and then decreases and finally increases and then decreases with increasing R600a mole fraction. When the R600a/R601a mole fraction is 0.7/0.3, the net power output of the system is maximal. The maximum net power output of the mixture system is 3.72% and 38.00% higher than that of the R601a and R600a systems, respectively.
- When the R600a/R601a mixtures are used as the working fluid in the IHE-OFC system, the net power output does not necessarily increase. When the R600a mole fraction is 0.0, 0.2-0.6, and 0.9-1, the net power output of IHE-OFC is greater than that of simple OFC. When the R600a mole fraction is 0.1 and 0.7-0.8, the net power output of IHE-OFC is less than that of simple OFC.
- The thermal efficiency of IHE-OFC has been significantly improved. When the R600a/R601a mole fraction is 0.7/0.3, the maximum thermal efficiency of IHE-OFC is 6.23%. The maximum relative increment of the IHE-OFC system is 10.98% compared with that of the simple OFC system.
- For R600a/R601a mixtures, when the R600a mole fraction is 0, the EGC of the IHE-OFC system is higher than that of the simple OFC system. When the R600a mole fraction is 0.1-1, the EGC of the IHE-OFC system is less than that of the simple OFC system.

Acknowledgment

This work was supported by Yunnan Provincial Department of Education Science Research Fund Project (Grant No. 2019J0025, 2018JS551), Talent Project of Yunnan Univer-

sity (Grant No.C176220200), Scientific Research Foundation of Kunming Metallurgy College (Grant No. Xxrcxm201802), and National Natural Science Foundation Programs of China (Grant Nos. 51736005, 51878591).

Nomenclature

g – gravitational acceleration, (= 9.8 m/s^2)
H – pressure head, [m]
h – specific enthalpy, [kJkg^{-1}]
$\dot{m}$ – mass-flow rate, [kgs^{-1}]
P – pressure, [MPa]
Q – heat absorption capacity, [kW]
Q_i – heat transfer through a surface, [kW]
s – specific entropy, [kJK^{-1}kg^{-1}]
T – temperature, [°C]
ΔT – temperature diffidence, [°C]
W – power, [kW]
x – vapor dryness

Greek symbol

η – efficiency, [%]

Subscripts

1-11 – state points
c – condenser
cri – critical
cool – cooling water
cw – cold working fluid
dew – dew point
F – flasher
f – working fluid
H – heater
HS – heat source
in – inlet
l – liquid fraction
net – net power output
out – outlet
p – feed pump
sys – system
T – turbine
v – vapor fraction

Acronyms

ACC – annual capital cost
AOC – annual operation costs
EGC – electricity generation costs
GWP – global warming potential
IHE – internal heat exchange
ODP – ozone depletion potential
OFC – organic flash cycle
ORC – organic Rankine cycle
PEC – purchased equipment costs

References

[1] Ge, Z., *et al.*, Thermodynamic Analysis of Dual-Loop Organic Rankine Cycle Using Zeotropic Mixtures for Internal Combustion Engine Waste Heat Recovery, *Energy Conversion and Management*, *166* (2018), 6, pp. 201-214
[2] Yang, F. F., *et al.*, On the Temperature Dependence of the α Function in the Cubic Equation of State, *Chemical Engineering Science*, *192* (2018), 8, pp. 565-575
[3] Liu, H. D., *et al.*, Multi-Objective Optimization of Fin-and-Tube Evaporator for a Diesel Engine Organic Rankine Cycle (ORC) Combined System Using Particle Swarm Optimization Algorithm, *Energy Conversion and Management*, *151* (2017), 11, pp. 147-157
[4] Yang, F. F., *et al.*, The Cubic-Plus-Association Equation of State for Hydrofluorocarbons, Hydrofluoroolefins, and their Binary Mixtures, *Chemical Engineering Science*, *209* (2019), 12, 115182
[5] DiPippo, R., *Geothermal Power Plants: Principles, Applications, and Case Studies*, Elsevier, Oxford, UK, 2005, pp. 772-773
[6] Liu, Q., *et al.*, Performance Analyses of Geothermal Organic Rankine Cycles with Selected Hydrocarbon Working Fluids, *Energy*, *63* (2013), 12, pp. 123-132
[7] Ho, T., *et al.*, Comparison of the Organic Flash Cycle (OFC) to other Advanced Vapor Cycles for Intermediate and High Temperature Waste Heat Reclamation and Solar Thermal Energy, *Energy*, *42* (2012), 6, pp. 213-223
[8] Lee, H. Y., *et al.*, Comparative Analysis of Thermodynamic Performance and Optimization of Organic Flash Cycle (OFC) and Organic Rankine Cycle (ORC), *Applied Thermal Engineering*, *100* (2016), 5, pp. 680-690
[9] Mondal, S., *et al.*, Power by Waste Heat Recovery from Low Temperature Industrial Flue Gas by Organic Flash Cycle (OFC) and Transcritical-CO_2 Power Cycle: A Comparative Study Through Combined Thermodynamic and Economic Analysis, *Energy*, *121* (2017), 2, pp. 832-840
[10] Mosaffa, A. H., *et al.*, Proposal and Thermoeconomic Analysis of Geothermal Flash Binary Power Plants Utilizing Different Types of Organic Flash Cycle, *Geothermics*, *72* (2018), 5, pp. 47-63

[11] Ho, T., *et al.*, Increased Power Production through Enhancements to the Organic Flash Cycle (OFC), *Energy, 45* (2012), 9, pp. 686-695
[12] Varma, G.V.P, *et al.* Power Generation from Low Temperature Heat Recovery [J], *Renewable and Sustainable Energy Reviews, 75* (2016), Aug., pp. 402-414
[13] Li, Z., *et al.* Comparison Study of Trilateral Rankine Cycle, Organic Flash Cycle and basic Organic Rankine Cycle for Low Grade Heat Recovery [J], *Energy Procedia, 142* (2017), Dec., pp. 1441-1447
[14] Kishimoto, A., *et al.*, Study of the Flash Cycle Using Liquid Heat Recirculation (FC-LHR) for Energy Saving in Industry, *Chemical Engineering Transactions, 24* (2014), 12, pp. 1-6
[15] Mondal, S., *et al.*, Waste Heat Recovery through Organic Flash Cycle (OFC) Using R245fa–R600 Mixtures as the Working Fluid, *Clean Technologies and Environmental Policy, 21* (2019), 10, pp. 1575-1586
[16] Li, J., *et al.*, Effects of Heat Source Temperature and Mixtures Composition on the Combined Superiority of Dual-Pressure Evaporation Organic Rankine Cycle and Zeotropic Mixtures, *Energy, 174* (2019), 5, pp. 436-449
[17] Liu, Q., *et al.*, Effect of Condensation Temperature Glide on the Performance of Organic Rankine Cycles with Zeotropic Mixtures Working Fluids, *Applied Energy, 115* (2014), 2, pp. 394-404
[18] Wang, Y. P., *et al.*, Experimental Investigation on the Performance of ORC Power System Using Zeotropic Mixture R601a/R600a [J], *International Journal of Energy Research, 41* (2017), 5, pp. 673-688
[19] Liu, Q., *et al.*, Parametric Optimization and Performance Analyses of Geothermal Organic Rankine Cycles Using R600a/R601a Mixtures as Working Fluids, *Applied Energy, 148* (2015), 6, pp. 410-420
[20] Zhu, J. L., *et al.*, Parametric Optimization of Organic Rankine cycle with R245fa/R601a as Working Fluid, *Transactions of Tianjin University, 21* (2015), 1, pp. 69-75
[21] Li, T. L., *et al.*, Experimental Comparison of R245fa and R245fa/R601a for Organic Rankine Cycle Using Scroll Expander, *Energy research, 39* (2015), 2, pp. 202-214
[22] Li, J., *et al.*, Performance Analyses and Improvement Guidelines for Organic Rankine Cycles Using R600a/R601a Mixtures Driven by Heat Sources of 100 °C to 200 °C, *International Journal of Energy Research, 43* (2019), 2, pp. 905-920
[23] Li, W., *et al.*, Effects of Evaporating Temperature and Internal Heat Exchanger on Organic Rankine Cycle, *Applied Thermal Engineering, 31* (2011), 12, pp. 4014-4023
[24] Li, T, L., *et al.*, Performance Analysis and Improvement of Geothermal Binary Cycle Power Plant in Oilfield, *Journal of Central South University, 20* (2013), 2, pp. 457-465
[25] Yang, F. B., *et al.*, Performance Analysis of Waste Heat Recovery with a Dual Loop Organic Rankine Cycle (ORC) System for Diesel Engine Under Various Operating Conditions, *Energy Conversion and Management, 80* (2014), 4, pp. 243-255
[26] Lu, J. L., *et al.*, Analysis of Organic Rankine Cycles Using Zeotropic Mixtures as Working Fluids Under Different Restrictive Conditions, *Energy Conversion and Management, 126* (2016), 10, pp. 704-716
[27] Steven, L., *et al.*, Review of Organic Rankine Cycle (ORC) Architectures for Waste Heat Recovery, *Renewable and Sustainable Energy Reviews, 47* (2015), 7, pp. 448-461
[28] Yang, F. B., *et al.*, Thermo-Economic Multi-Objective Optimization of an Organic Rankine Cycle for Exhaust Waste Heat Recovery of a Diesel Engine, *Energy, 93* (2015), 6, pp. 2208-2228
[29] Heberle, F., *et al.*, Zeotropic Mixtures as Working Fluids in Organic Rankine Cycles for Low-Enthalpy Geothermal Resources, *Renew Energy, 37* (2012), 6, pp. 364-370
[30] Lecompte, S., *et al.*, Exergy Analysis of Zeotropic Mixtures as Working Fluids in Organic Rankine Cycles, *Energy Conversion and Management, 85* (2014), 9, pp. 727-739
[31] Li, J., *et al.*, Performance Analysis of Organic Rankine Cycle Using R600a/R601a Mixtures with Liquid-Separated Condensation, *Applied Energy, 190* (2017), 6, pp. 376-389
[32] Mondal, S., *et al.*, Performance Assessment of a Low Grade Waste Heat Driven Organic Flash Cycle (OFC) with Ejector, *Energy, 163* (2018), 11, pp. 849-862

Paper submitted: May 7, 2020
Paper revised: June 15, 2020
Paper accepted: September 21, 2020
© 2021 Society of Thermal Engineers of Serbia.
Published by the Vinča Institute of Nuclear Sciences, Belgrade, Serbia.
This is an open access article distributed under the CC BY-NC-ND 4.0 terms and conditions.